THESIS FOR THE DEGREE OF LICENTIATE OF ENGINEERING

Non-invasive EEG Functional Neuroimaging for Localizing Epileptic Brain Activity

by

YAZDAN SHIRVANY

CHALMERS

Department of Signals and Systems
CHALMERS UNIVERSITY OF TECHNOLOGY
Göteborg, Sweden 2012

Göteborg 2012

Non-invasive EEG Functional Neuroimaging for Localizing Epileptic Brain Activity
YAZDAN SHIRVANY

This thesis has been prepared using LaTeX.

Licentiatavhandling vid Chalmers Tekniska Högskola
Ny serie nr R002/2012
ISSN 1403-266X

Department of Signals and Systems
Signal Processing Group
Chalmers University of Technology
SE-412 96 Göteborg, Sweden

Phone: +46 (0)31 772 1716
Fax: +46 (0)31 772 1725
E-mail: yazdan.shirvany@chalmers.se

Front cover: Credit @psdesign1 - Fotolia.com.

Printed by Chalmers Reproservice
Göteborg, Sweden, February 2012

If we knew what it was we were doing,
it would not be called research, would it?
A. Einstein (1879-1955)

Abstract

Surgical therapy has become an important therapeutic alternative for patients with medically intractable epilepsy. Correct and anatomically precise localization of the epileptic focus, preferably with non-invasive methods, is the main goal of the pre-surgical epilepsy diagnosis to decide if resection of brain tissue is possible. The most important diagnosis tool used at epilepsy surgery centers is electroencephalography (EEG), which is used to find the source of activities inside the brain by measuring the voltage potential on the scalp with the EEG electrodes at different locations. The overall goal is to develop a non-invasive, clinically-viable, time-efficient method for localization of epileptic brain activity based on EEG source localization. We propose a new global optimization method based on particle swarm optimization (PSO) to solve the epileptic spike EEG source localization inverse problem. In the forward problem a modified subtraction method is used for modeling the dipole source to reduce the computational time. The new proposed inverse method is tested for synthetic and real EEG data and the results are compared with other existing methods. The results for synthetic data showed that the new PSO algorithm can find the optimal solution significantly faster and more accurate than the other methods and also reduce the probability of trapping in local minima. In the clinical test, somatosensory evoked potentials (SEPs) were measured for a healthy subject and used for source localization. A realistic 1 *mm* patient-specific, isotropic finite element model of the subject's head with special consideration of precise modeling the two compartments, skull and cerebrospinal fluid (CSF), was generated using T1-weighted magnetic resonance imaging data. The proposed inverse problem solver found the global minima with acceptable accuracy and reasonable number of iterations.

Preface

This thesis is in partial fulfillment of the requirements for the degree of Licentiate of Engineering at Chalmers University of Technology, Göteborg, Sweden.

The work has been performed in the Biomedical Electromagnetics Group, Department of Signals and Systems at Chalmers between Jan. 2009 and Mar. 2012 under the supervision of Professor Mikael Persson, Associate Professor Fredrik Edelvik (Fraunhofer-Chalmers Research Center, FCC) and Medical Doctor Anders Hedström (Sahlgrenska University Hospital). Prof. Persson also acts as examiner of the thesis. In addition to the supervisors, Dr. Stefan Jakobsson has been involved in this work.

This work has been supported in part by Chalmers University of Technology and Islamic Development Bank. The project has been performed in collaboration with industry, namely FCC. The data for this thesis was recorded by the Neurophysiology Department, Sahlgrenska University Hospital, Göteborg, Sweden.

List of Publications

This thesis is based on the following papers:

Paper I
Yazdan Shirvany, Fredrik Edelvik, Stefan Jakobsson, Anders Hedström, Mikael Persson, "Application of Particle Swarm Optimization in Epileptic Spike EEG Source Localization", *Submitted*.

Paper II
Yazdan Shirvany, Fredrik Edelvik, Stefan Jakobsson, Anders Hedström, Qaiser Mahmood, Artur Chodorowski, Mikael Persson. "A Clinical Study of EEG Source Localization: Somatosensory Evoked Potential", *Manuscript*.

Other related publication by the author not included in this thesis:

1. Fredrik Edelvik, Björn Andersson, Stefan Jakobsson, Stig Larsson, Mikael Persson, and **Yazdan Shirvany**. "An improved method for dipole modeling in EEG-based source localization". *World Congress on Medical Physics and Biomedical Engineering, September 7 - 12, 2009, Munich, Germany, volume 25/9 of IFMBE Proceedings, pages 146 - 149*. Springer Berlin Heidelberg, 2009.

2. Mikael Persson, Tomas McKelvey, Andreas Fhager, Hoi Shun Lui, **Yazdan Shirvany**, Artur Chodorowski, Qaiser Mahmood, Fredrik Edelvik, Magnus Thordstein, Anders Hedström and Mikael Elam, "Advances in Neuro Diagnostic based on Microwave Technology, Transcranial Magnetic Stimulation and EEG source localization", *Asia Pacific Microwave Conference*.

3. **Yazdan Shirvany**, Mikael Persson, Fredrik Edelvik, Stefan Jakobsson, Anders Hedström, Koushyar Kowkabzadeh, Antonio Reyes and Hoi Shun Lui. " Dipole Source localization based on Epileptic Spike Signals and Particle Swarm Optimization method in the Finite Element Head Model", *Proceedings of Medicinteknikdagarna 2010*, pp. 128.

4. Antonio Reyes, Koushyar Kowkabzadeh, **Yazdan Shirvany**, Hoi Shun Lui, Simon Bergstrand, Anders Hedström and Mikael Persson, "Evaluations of Brain Tissue Segmentation from the Widely-Used Software Packages", *Proceedings of Medicinteknikdagarna 2010*, pp. 187.

Acknowledgments

I would like to express my sincere gratitude to my supervisors for their time and patience. First of all, I express my sincere thanks to Prof. Mikael Persson for his support and patience. I would also like to express my thankfulness to my co-supervisor Assoc. Prof. Fredrik Edelvik from FCC for all his kindness and time he dedicated to the progress of my research articles. I am very grateful to Dr. Anders Hedström and Prof. Mikael Elam from Sahlgrenska University Hospital for their valuable feedback and enthusiasm with pushing this work towards clinics. I also want to thank all the other nice members involved in this project, Dr. Stefan Jakobsson, Dr. Artur Chodorowski, Dr. Andrew Mehnert, M.Sci. Simon Bergstrand, and M.Sci. Qaiser Mahmood.

I would like to thank my friends for all their support and kindness. Here I say thanks to my lovely brother Reza who always be with me. Lot of thanks to Mahdieh for all her support. My special thanks to Oskar, who is my colleague, friend and ski teacher and also thanks to Sajed, my gym mate. Thanks to Nima, Sima, Tony, Hoi-Shun, Xuezhi and all other my lovely friends that create an unforgettable time in my life. Last but not least, I would like to mention the unfailing support of my parents, bigger brother, Ramin, and lovely sister, Roshan. Thanks to all of you.

Contents

Part I
Extended Summary

CHAPTER 1

Introduction

Epilepsy is one of the most common neurologic diseases in the world, and is present in up to 4% of the world's population. Many patients with epilepsy never receive the treatment which make them seizure free; consequently, treatment of epilepsy with medications is a major effort of the World Health Organization [1]. Surgical therapy has become an important therapeutic alternative for patients with medically intractable epilepsy.

Although intracranial surgery involves inherent risks, these risks do not equal the risks of uncontrolled seizures. The morbidity and mortality of seizures include the following [1]:

- Accidental injury, commonly include fractures, burns, dental injuries, lacerations, and head injuries.
- Cognitive decline and memory loss, which over time has been demonstrated to occur in patients.
- Sudden unexplained death in epilepsy (SUDEP) that can reach a rate of one death per 500 patients per year.
- Psychological, social, and vocational impairment.

From the above factors, clearly a continued medical therapy after failure to control seizures with several trials of antiepileptic drugs (AEDs) is not effective treatment. Moreover, Engel in [2] shows that the benefits of anteromedial temporal lobe resection (AMTR) for disabling complex partial seizure is greater than continued treatment with AEDs, and the risks are at least comparable. In addition, surgery

yields a better quality of life and reduced depression and anxiety as early as 3 months after temporal resection, compared with continued medical therapy [3].

The heterogeneity of focal epilepsy across patients demands an extensive multimodal approach to focus localization [4]. Generally, results of at least three standard investigative modalities, conducted in series, are required to concur before surgery can be planned. Standard modalities are: reported clinical seizure semiology; electroencephalography (EEG) or electrocorticography (ECoG) seizure onset location combined with videoderived seizure semiology; structural MRI (sMRI); and nuclear imaging techniques. Nuclear imaging detects abnormality in ictal versus interictal blood flow by single photon emission computed tomography (SPECT), and/or abnormality in interictal glucose metabolism by positron emission tomography (PET). The localization performance of these methods is validated by comparison with post-surgical outcomes.

Only when a well-defined structural lesion agrees with seizure semiology and scalp EEG onset with or without radiotracer techniques, can surgery be planned without invasive study. sMRI locates brain lesions in about 70-80% of focal epilepsy [5]. In the remainder, intracranial electrode placement is considered. When the lesion is located, but is close to eloquent cortex, fMRI and invasive studies help minimise resection of such tissue. However, a visualised lesion may not represent the entire seizure-generating region. Underestimating the extent of the region can result in the re-occurrence of seizures following resective surgery. Overestimating the extent of the region holds an increased risk of functional deficits. Correct and anatomically precise localization of the epileptic focus, preferably with non-invasive methods, is the main goal of the pre-surgical epilepsy diagnosis. The current techniques have limited accuracy and are therefore associated with significant risks. Hence, there is a need for improved, complementary, time-efficient, non-invasive methods to define the seizure-generating focus.

The EEG is the most important diagnosis tool used at epilepsy surgery centers. This method localize epileptic electrical activity, called spike waveforms. Spikes occur between seizure times and are closely linked to the site of seizure focus. In contrast to seizures, spikes do not cause patient movement artifact in an MRI scanner, which is advantageous to data acquisition.

The brain activity is often modeled as a current dipole. It is shown in [6] that this current dipole is an acceptable approximation for modeling the neural activities in the brain. The current dipole represents a focal area of synchronously active pyramidal cells located in the gery matter cortex, see Chapter 2. Source localization is heavily dependent on the choice of dipole model and several different alternatives have been suggested in the literature [7, 8]. Also the localization accuracy is affected by different factors including, head-modeling error, EEG signal noise and electrode displacements as well as the numerical computational error. A major limitation in EEG-based source reconstruction has been the poor spatial

accuracy, which is attributed to low resolution of previous EEG systems and to the use of simplified spherical head models for solving the inverse problem.

The procedure of the EEG source localization deals with two problems. First, the forward problem to find the scalp potentials for the given current dipole(s) inside the brain and second the inverse problem to estimate the source(s) that fits with the given potential distribution at the scalp electrodes. Thus, source localization requires an accurate solution of the inverse problem with a realistic computational effort for the forward problem. EEG-based source localization is an active field of research [9, 10], but partly due to the mentioned shortcomings the computational techniques are not yet part of the standard pre-surgical diagnostic workup.

1.1 Overview of the thesis

Chapter 2 gives a short introduction to the physics of EEG. Chapter 3 introduces the forward problem. Chapter 4 describes the inverse problem and its mathematical formulation. Chapter 5 explains the particle swarm optimization method and some proposed modifications in detail. Chapter 6 deals with the numerical results of EEG source localization for the synthetic and real models. The contribution and future work are presented in Chapter 7. Part **II** includes Paper **I** which is submitted for publication and Paper **II** which is in manuscript.

CHAPTER 2

The physics of EEG

In this section the physiology of the EEG will be shortly described. It is important to know the underlying mechanisms of the EEG. Moreover, forward modeling also needs a good model for the generators of the EEG.

2.1 Neurophysiology

The brain consists of about 10^{10} nerve cells or neurons. Neurons are capable of generating and transmitting electrochemical impulses. There are many different kinds of neurons, but they all have the same basic structure. The **soma** or **cell body** contains the nucleus of the cell and is essential for the continuing life of the neuron. The **dendrites**, arising from the soma, are specialized in receiving inputs from other nerve cells; a neuron may have several dendrites. Via the **axon**, impulses are sent to other neurons; a neuron has only one axon. The axon's end is divided into branches which form **synapses** with other neurons, see Figure 2.1.

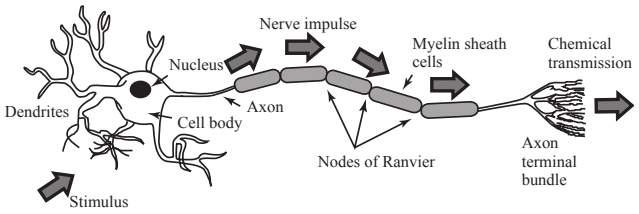

Figure 2.1: Structure of a neuron (adopted from Attwood and MacKay [11])

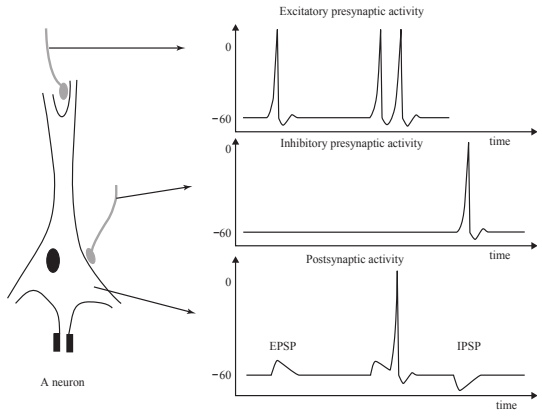

Figure 2.2: The neuron membrane potential changes and current flow during synaptic activation recorded by means of intracellular microelectrodes. Action potentials in the excitatory and inhibitory presynaptic fibre respectively lead to EPSP and IPSP in the postsynaptic neuron (adopted from Saeid Sanei and J.A. Chambers [14])

The synapse is a specialized interface between two nerve cells. The synapse consists of a cleft between a pre-synaptic and post-synaptic neuron. At a synapse, between the axon of one neuron and the dendrite or cell body of the next neuron, impulse transmission depends upon chemicals called neurotransmitters. Further readings on the anatomy of the brain can be found in [12, 13].

At rest the intracellular environment of a neuron is negatively polarized at approximately -70 mV compared with the extracellular environment. The potential difference is due to an unequal distribution of Na+, K+ and Cl- ions across the cell membrane. This unequal distribution is maintained by the Na+ and K+ ion pumps located in the cell membrane. The neuron's task is to process and transmit signals. This is done by an alternating chain of electrical and chemical signals. Active neurons secrete a neurotransmitter, which is a chemical substance, at the synaptical site. The synapses are mainly localized at the dendrites and the cell body of the post-synaptic cell. The neurotransmitter in contact with the receptors changes the permeability of the membrane for charged ions. Many synapses are termed excitatory, because the neurotransmitter causes the post-synaptic neuron to depolarize (become more negative outside as Na+ ions enter the cell) and transmit an electrical impulse to another neuron, muscle cell, or gland. In other words, depolarization means that the potential difference between the intra- and extracellular environment decreases. Instead of -70 mV the potential difference becomes -40 mV. This depolarization is also called an excitatory post-synaptic potential (EPSP). On the other hand some synapses, however, are inhibitory, meaning that the neurotransmitter causes the post-synaptic neuron to hyperpolarize (become

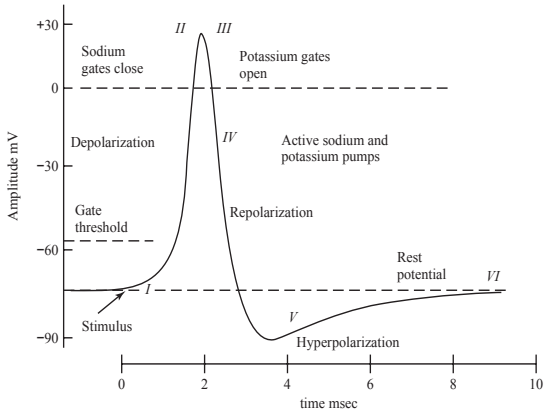

Figure 2.3: Changing the membrane potential for a giant squid axon by closing the Na channels and opening K channels (adopted from Ka Xiong Charand [17])

even more positive outside as K+ ions leave the cell or Cl- ions enter the cell) and therefore not transmit an electrical impulse. This potential change is also called an inhibitory post-synaptic potential (IPSP). There are a large number of synapses from different pre-synaptic neurons in contact with one post-synaptic neuron. Figure 2.2 shows the membrane changes recorded by means of intracellular microelectrodes. At the cell body all the EPSP and IPSP signals are integrated. When a net depolarization of the intracellular compartment at the cell body reaches a certain threshold, an action potential is generated. Figure 2.3 shows an example of above activities schematically for a giant squit axon. An action potential then propagates along the axon to other neurons [15, 16].

2.2 The generators of the EEG

One neuron generates a small amount of electrical activity. This small amount cannot be picked up by surface electrodes, as it is overwhelmed by other electrical activity from neighboring neuron groups. When a large group of neurons is simultaneously active, the electrical activity is large enough to be picked up by the electrodes at the surface and thus generating the EEG. The electrodes used in scalp EEG are large and remote. They only detect summed activities of a large number of neurons which are synchronously electrically active. The action potentials can be large in amplitude ($70-110\ mV$) but they have a short duration (0.3 ms). A synchronous firing of action potentials of neighboring neurons is unlikely. The post-synaptic potentials are the generators of the extracellular potential field which can be recorded with an EEG. Their time course is larger ($10-20\ ms$)

which enables summed activity of neighboring neurons. However their amplitude is smaller ($0.1-10\ mV$) [18, 16].

CHAPTER 3

Forward Problem

3.1 Poisson's Equation

As mentioned in Chapter 2, the EEG reflects the electrical activity of a subgroup of neurons, especially pyramidal neuron cells, where the apical dendrite is systematically oriented orthogonal to the brain surface. The characteristic frequencies of the signals in the kHz range and below make the capacitive and inductive effects of the tissue negligible. Therefore, the quasi-static approximation of Maxwell's equations for the potential Φ can be used. It can be assumed that μ is constant over the whole volume and is equal to the permeability of vacuum [19]. Therefore, the electric and magnetic fields can be described by the quasi-static Maxwell equations,

$$\nabla \cdot \mathbf{D} = \rho, \tag{3.1}$$
$$\nabla \times \mathbf{E} = 0, \tag{3.2}$$
$$\nabla \times \mathbf{B} = \mu \mathbf{j}, \tag{3.3}$$
$$\nabla \cdot \mathbf{B} = 0, \tag{3.4}$$

with the constitutive equations,

$$\mathbf{D} = \varepsilon \mathbf{E}, \tag{3.5}$$
$$\mathbf{B} = \mu \mathbf{H}. \tag{3.6}$$

The irrotational nature of **E** indicate by (3.2) enables us to define a scalar electric potential Φ, as follows:

$$\mathbf{E} = -\nabla\Phi \tag{3.7}$$

The current density is generally divided into two parts [19], the so-called primary or source current, $\mathbf{j}^s$, and the secondary or return currents, $\sigma\mathbf{E}$,

$$\mathbf{j} = \mathbf{j}^s + \sigma\mathbf{E} \tag{3.8}$$

where σ denotes the 3×3 conductivity tensor. Here, the source currents $\mathbf{j}^s$, are movements of ions within the dendrites of the large pyramidal cells of activated regions in the cortex sheet of the human brain. If we denote the domain of interest as Ω (with boundary $\partial\Omega$), taking the divergence of Eq. (3.3) (divergence of a curl of a vector is zero) and using equations (3.7) and (3.8) give the Poisson's equation

$$\nabla\cdot(\sigma\nabla\Phi) = \nabla\cdot\mathbf{j}^s \text{ in } \Omega, \tag{3.9}$$

subject to the conditions

$$\hat{\mathbf{n}}\cdot(\sigma\nabla\Phi) = 0 \text{ on } \partial\Omega, \tag{3.10a}$$

$$\Phi(\mathbf{x}_{\text{ref}}) = 0. \tag{3.10b}$$

Various modeling possibilities for the primary currents are discussed in the literature [20, 21, 22, 23]. We will restrict ourselves to the mathematical dipole model. Here we explain the modified subtraction method briefly. Paper **I** presents the solution of Poisson's equation in detail.

Assume a source current $\mathbf{j}^s$ as a mathematical dipole placed at position $\mathbf{x}_0 \in \Omega$ with the moment $\mathbf{M} \in \mathbf{R}^3$,

$$\mathbf{j}^s(\mathbf{x}) = \delta(\mathbf{x}-\mathbf{x}_0)\mathbf{M}. \tag{3.11}$$

This source model has a singularity at $\mathbf{x}_0$ and is therefore difficult to model with standard finite elements. A Modified subtraction method [7, 8] is used to circumvent this problem, where the total potential is split into two parts,

$$\Phi = \chi\Phi^\infty + \Phi^{\text{mod}} = F^\infty + \Phi^{\text{mod}}. \tag{3.12}$$

For convenience, we have defined the function

$$F^\infty = \chi\Phi^\infty. \tag{3.13}$$

The first part, Φ^∞, is the solution to Eq. (3.9) in an unbounded domain with con-

stant conductivity σ^{∞},

$$\Delta\Phi^{\infty} = \frac{\nabla \cdot \mathbf{j}^{s}}{\sigma^{\infty}}. \tag{3.14}$$

The solution can in this case be formed analytically as

$$\Phi^{\infty}(\mathbf{x}) = \frac{1}{4\pi\sigma^{\infty}} \frac{(\mathbf{x}-\mathbf{x}_0)\cdot\mathbf{M}}{|\,\mathbf{x}-\mathbf{x}_0\,|^3}. \tag{3.15}$$

For future references, we notice that both the source current $\mathbf{j}^{s}$ and Φ^{∞} depend linearly on the dipole moment $\mathbf{M}$. χ is a smooth cut-off function which is identically 1 in a neighborhood of $\mathbf{x}_0$. Using Eqs. (3.12) and (3.9), the new formulation reads,

$$-\nabla \cdot \left(\sigma \nabla \Phi^{\mathrm{mod}}\right) = \nabla \cdot (\sigma \nabla F^{\infty}) - \nabla \cdot \mathbf{j}^{s} \text{ in } \Omega, \tag{3.16}$$

subject to the conditions

$$\hat{\mathbf{n}} \cdot \left(\sigma \nabla \Phi^{\mathrm{mod}}\right) = -\hat{\mathbf{n}} \cdot (\sigma \nabla F^{\infty}) \text{ on } \partial\Omega, \tag{3.17a}$$

$$\Phi(\mathbf{x}_{\mathrm{ref}}) = 0. \tag{3.17b}$$

3.2 Finite Element Method

There are several numerical methods to solve Eq. (3.16), e.g., Finite Element Method, Boundary Element Method and Finite Difference Method, for more information see [9]. For the forward problem we use a FEM solver which is developed by the Fraunhofer-Chalmers Research Center based on a modified subtraction method [8] for modeling the dipole source.

Apply standard FE method to the Eq. (3.16) for the EEG forward problem yield a linear equation system,

$$\mathbf{K}\mathbf{u}^{\mathrm{mod}} = \mathbf{b}, \tag{3.18}$$

where $\mathbf{K} \in R^{N\times N}$ is a sparse symmetric positive definite stiffness matrix, $\mathbf{u}^{\mathrm{mod}} \in R^{N}$ the coefficient vector of the modified electric potential and $\mathbf{b} \in R^{N}$ the right hand side vector with N being the number of FE nodes.

In EEG applications the potentials are typically measured at approximately 40 to 100 electrodes. Then the values of the potential at the electrodes can be obtained by multiplying the vector of nodes values with a *restriction matrix* $\mathbf{R}$

$$\mathbf{u}^{\mathrm{mod}}_{\mathrm{elec}} = \mathbf{R}\mathbf{u}^{\mathrm{mod}}. \tag{3.19}$$

The size of the matrix $\mathbf{R}$ is $N_{\text{elec}} \times N$. Since only the relative differences of the potential are of interest, it is common in EEG to use the average signal as a common reference, this is the so called *average reference montage*. Let $\overline{\mathbf{R}}$ be the transfer matrix such that

$$\mathbf{u}_{\text{elec}}^{\text{mod}} - \overline{\mathbf{u}}_{\text{elec}}^{\text{mod}} = \overline{\mathbf{R}}\mathbf{u}^{\text{mod}}, \tag{3.20}$$

where $\overline{\mathbf{u}}_{\text{elec}}$ is the average of the potential at all nodes. $\overline{\mathbf{R}}$ can be obtained from $\mathbf{R}$ by subtracting the column-wise mean from each entry. From the relation (3.18) we see that $\mathbf{u}^{\text{mod}} = \mathbf{K}^{-1}\mathbf{b}$ and therefore

$$\mathbf{u}_{\text{elec}}^{\text{mod}} - \overline{\mathbf{u}}_{\text{elec}}^{\text{mod}} = \overline{\mathbf{R}}\mathbf{u}^{\text{mod}} = \overline{\mathbf{R}}\mathbf{K}^{-1}\mathbf{b} = \overline{\mathbf{T}}\mathbf{b}. \tag{3.21}$$

We call $\overline{\mathbf{T}} = \overline{\mathbf{R}}\mathbf{K}^{-1}$ the *transfer matrix* for the average reference montage. The right hand side, $\mathbf{b}$, is linear in the dipole moment $\mathbf{M}$ and non-linear in dipole position $\mathbf{x}_0$, therefore we can write it as follow,

$$\mathbf{b} = \mathbf{b}(\mathbf{x}_0, \mathbf{M}) = \mathbf{B}(\mathbf{x}_0)\mathbf{M}, \tag{3.22}$$

In the modified subtraction method the contribution to the total potential comes from two parts. One part from the finite element method computed as described above and one direct contribution from Eq. (3.13). Both these contributions are linear in the dipole moment so therefore the total potential at the electrodes can be written

$$\mathbf{u}_{\text{elec}} = \left(\overline{\mathbf{T}}\mathbf{B}(\mathbf{x}_0) + \mathbf{F}_{\text{elec}}^{\infty}(\mathbf{x}_0)\right)\mathbf{M} = \mathbf{G}(\mathbf{x}_0)\mathbf{M}. \tag{3.23}$$

Here $\mathbf{F}_{\text{elec}}^{\infty}(\mathbf{x}_0)$ is the value of the function F^{∞} for the three polarizations at all electrodes when dipole is located at $\mathbf{x}_0$ and $\mathbf{G}(\mathbf{x}_0)$ is called the *gain matrix*. We use Eq. (3.23) in the inverse problem to find the position of the dipole.

CHAPTER 4

Inverse Problem

Localization of the neural activity inside the brain based on the scalp EEG signal is called the EEG inverse problem. Different inverse approaches for discrete and continuous source parameter space have been proposed [24], which could be divided into two groups, non-parametric and parametric methods. The main difference between these two methods is whether a fixed number of dipoles is assumed *a priori* or not. The non-parametric methods act on a distributed source model, where the restriction to a limited number of focal sources is removed. On the other hand parametric methods based on current dipole are well suited for estimating the well-localized activated neural sources for events like epileptic spike or early stage of a epileptic seizure [6]. For the clinical use, the EEG source localization method should be accurate (in a source estimation sense) as well as fast (in a computational sense). Here we use parametric methods for the epilepsy spike inverse problem. In this approach, a search is made for the best-fit dipole position(s) and orientation(s).

4.1 Parametric Method

Since the dimension of the space of possible source distributions is infinite and there are only a finite number of electrodes, the problem is underdetermined and has no unique solution. To attain uniqueness it is necessary to impose a priori knowledge on the source distribution. In a parametric method, the number of dipoles is assumed to be fixed and their locations and moments are chosen such that the potentials at the electrodes, $\mathbf{u}_{elec}$, that are computed in the forward prob-

lem, approximate the measured potentials $\mathbf{u}_{meas}$ well according to some criteria. Parametric Methods are also referred to as Equivalent Current Dipole Methods or Concentrated Source or Spatio-Temporal Dipole Fit Models. Here we follow the common practice and choose the parameters such that we have the best fit in least squares sense. For one dipole we get the following minimization problem

$$J = \min_{\substack{\mathbf{x}\in\Omega_{brain} \\ \mathbf{M}\in\mathbf{R}^d}} \| \mathbf{u}_{meas} - \mathbf{u}_{elec}(\mathbf{x},\mathbf{M}) \|, \tag{4.1}$$

where Ω_{brain} is the brain domain and d the dimension. Since this is a least squares problem and $\mathbf{u}_{elec}$ depends linearly on the dipole moment, see Eq. (3.23), it is convenient to separate the parameters in (4.1) and solve for the dipole moment $\mathbf{M}$ first. Define, for fixed $\mathbf{x} \in \Omega_{brain}$,

$$J(\mathbf{x}) = \min_{\mathbf{M}\in\mathbf{R}^d} \| \mathbf{u}_{meas} - \mathbf{G}(\mathbf{x})\mathbf{M} \| . \tag{4.2}$$

According to the normal equations for linear least squares problems, optimality is obtained for

$$\hat{\mathbf{M}}(\mathbf{x}) = (\mathbf{G}^T(\mathbf{x})\mathbf{G}(\mathbf{x}))^{-1}\mathbf{G}^T(\mathbf{x})\mathbf{u}_{meas}. \tag{4.3}$$

Substituting (4.3) into (4.2) yields after some manipulation

$$J(\mathbf{x}) \quad = \quad \left(\mathbf{u}_{meas}^T[\mathbf{I} - \mathbf{G}(\mathbf{x})(\mathbf{G}^T(\mathbf{x})\mathbf{G}(\mathbf{x}))^{-1}\mathbf{G}^T(\mathbf{x})]\mathbf{u}_{meas}\right)^{1/2}. \tag{4.4}$$

Now we can reduce (4.1) to a minimization problem only over the dipole position

$$J = \min_{\substack{c_{brain}(\mathbf{x})\leq 0, \\ \mathbf{x}\in\Omega_{brain}}} \mathbf{J}(\mathbf{x}), \tag{4.5}$$

where a constraint function c_{brain} is introduced to define the optimization domain, see Section *Constraints* in Paper **I** and **II**.

CHAPTER 5

Particle Swarm Optimization

5.1 Standard PSO

The Particle Swarm Optimization concept was first introduced by Kennedy and Eberhart [25, 26] in 1995 based on the social system behavior such as movement of the school of birds or the flock of fishes for finding food. Each individual in the swarm is called a particle. The $i-th$ particle of the swarm is represented by the vectors $\mathbf{X}_i$ for its position and $\mathbf{V}_i$ for its velocity. The particle has a memory to record the position of its previous best performance, personal best (*pbest*), in the vector $\mathbf{P}_i$ and the position of the best particle in the swarm, global best (*gbest*), which is recorded in the vector $\mathbf{P}_g$.The particle swarm optimization algorithm consists of, in each iteration, changing the velocity of each particle towards position of its best performance, $\mathbf{P}_i$, and the swarm best position, $\mathbf{P}_g$. Thus in the original version particles move according to the following formula:

$$\begin{cases} \mathbf{V}_i^{t+1} & = \mathbf{V}_i^t + c_1 Rand()(\mathbf{P}_i - \mathbf{X}_i^t) \\ & \quad + c_2 Rand()(\mathbf{P}_g - \mathbf{X}_i^t), \\ \mathbf{X}_i^{t+1} & = \mathbf{X}_i^t + \mathbf{V}_i^{t+1}. \end{cases} \tag{5.1}$$

Parameters c_1 and c_2 are the *cognitive* and *social learning rates*. These two rates control the relative influence of the memory of the swarm's best performance to the memory of the individual and are often selected to the same value to give each learning rate equal weight. In addition to the c_1 and c_2 parameters, implementation of the original algorithm also requires placing limits on the search area ($\mathbf{X}_{max}$

and $\mathbf{X}_{min}$), and the velocity ($\mathbf{V}_{max}$).

Shi and Eberhart [27, 28] devised an inertia weight, *w*, to improve the accuracy of PSO by damping the velocities over time, allowing the swarm to converge with greater precision. By integration of *w* into the algorithm, the formula for computing the new velocity is

$$\begin{aligned}\mathbf{V}_i^{t+1} = w\mathbf{V}_i^t + c_1 Rand()(\mathbf{P}_i - \mathbf{X}_i^t) \\ + c_2 Rand()(\mathbf{P}_g - \mathbf{X}_i^t).\end{aligned} \tag{5.2}$$

As originally developed, *w* often is decreased linearly from about 0.9 to 0.4 during a search. Suitable selection of the inertia weight provides a balance between global and local exploration and exploitation, and the result is fewer iteration on average to find a sufficiently optimal solution [28].

In [29] Clerc derived a *constraint coefficient*, *K*, a modification of PSO and in [30] it was found that *K* combined with constraints on $\mathbf{V}_{max}$ significantly improved the PSO performance. The formula for computing the new velocity with constriction factor *K* is

$$\begin{aligned}\mathbf{V}_i^{t+1} = K(\mathbf{V}_i^t + c_1 Rand()(\mathbf{P}_i - \mathbf{X}_i^t) \\ + c_2 Rand()(\mathbf{P}_g - \mathbf{X}_i^t)),\end{aligned} \tag{5.3}$$

where $K = \frac{2}{|2-\phi-\sqrt{\phi^2-4\phi}|}$ and $\phi = c_1 + c_2 > 4$. This PSO is usually known as standard PSO (SPSO).

The PSO needs to select various different parameters, such as c_1, c_2, swarm size and neighborhood size etc. Selecting the best value for each parameter in the specific problem at hand may be a problematic and difficult task. For more details about the PSO parameter selection the reader is referred to [28]. The remedy is to make an adaptive PSO, which could adapt its behavior during the searching progress. In [31] and [29] a PSO algorithm with adaptive swarm size and swarm gravity center (the ”queen”) was introduced. These two modifications help to improve the convergence.

One way to avoid PSO to trap in local minima is mutation and using evolutionary programming (EP). In [32] EP with the concept of the evolving elite group was introduced. In this method *M* particles are selected among the swarm population by the *q*-tournament selection method as elite particles and then mutated by the EP method. By evaluating the fitness value of all the particles, the global best position is determined. For each particle, the nearest elite particle is determined by the Euclidean distance. The velocity and the position of the particle are updated according to the global best position, the nearest elite position, and the

personal best position. These are applied to PSO with inertia weight as follows:

$$\mathbf{V}_i^{t+1} = w\mathbf{V}_i^t + c_1 Rand()(\mathbf{P}_i - \mathbf{X}_i^t) + c_2 Rand()(\mathbf{P}_g - \mathbf{X}_i^t) + c_3 Rand()(\mathbf{P}_e - \mathbf{X}_i^t), \quad (5.4)$$

where c_3 denotes the constant of the nearest elite and $\mathbf{P}_e$ the nearest elite position.

5.2 Modified PSO

Here we use PSO with adaptive swarm size, adaptive neighborhood size, and the queen concept mixed with EP for EEG source localization. In addition, based on our observation of PSO behavior in the EEG source localization problem some modifications are proposed which help to speed up convergence and fulfill the problem constraints.

5.2.1 Concept of Authority

In our modified PSO (MPSO) we use the concept of authority and apply it to the particle's behavior. It means that in some steps the particles which are closer to the global best can influence the swarm performance and swarm decision more than other particles. This is because when the *gbest* particle is moving close to the minima, it cannot move faster than its velocity weight which is a small value during the last iterations. When PSO comes close to a minima (local or global) it can only find the global one when it has sufficiently many particles around *gbest*. Thus, PSO needs a lot of iterations to gather enough particles around *gbest*.

We extract the $R = 5$ closest particles to the *gbest* and let them fly freely based on their memory and knowledge. This allows the PSO to have more information around *gbest* before lots of particles come close to it and stuck with each other. Now, the velocity update is divided into two parts as

$$\mathbf{V}_i^{t+1} = w\mathbf{V}_i^t + c_1 Rand()(\mathbf{P}_i - \mathbf{X}_i^t) + c_2 Rand()(\mathbf{P}_g - \mathbf{X}_i^t) + c_3 Rand()(\mathbf{P}_e - \mathbf{X}_i^t), \quad (5.5)$$

where $i = 1, 2, ..., N - R$ and

$$\mathbf{V}_i^{t+1} = w\mathbf{V}_i^t + c_1 Rand()(\mathbf{P}_i - \mathbf{X}_i^t) \quad (5.6)$$

where $r = N - R + 1, ..., N$. The R nearest particles to *gbest* are re-selected in each iteration to ensure that the particles which moved away from the *gbest* loose their authority and update their velocity based on Eq. (5.5). The following parameters are selected for the MPSO coefficients: w = linear from 0.9 to 0.4, c_1 = 0.8, c_2 =

0.4, c_3 = 0.8 and swarm size = 30. In Paper **I** we evaluate the MPSO with synthetic data and compare it with some other methods.

CHAPTER 6

Numerical Results

6.1 Synthetic Model

To test the ability for EEG source localization we set up simulation experiments and then compare the MPSO with the SPSO and a global optimization method called DIRECT.

The DIRECT optimization algorithm was first introduced in [33]. It was created in order to solve difficult global optimization problems with bound constraints and a real-valued objective function. DIRECT is a sampling algorithm. That is, it requires no knowledge of the objective function gradient. Instead, the algorithm samples points in the domain, and uses the information it has obtained to decide where to search next. The DIRECT algorithm will globally converge to the minimal value of the objective function [33]. But this global convergence may come at the expense of a large and exhaustive search over the domain. The name DIRECT comes from the shortening of the phrase ”DIviding RECTangles”, which describes the way the algorithm moves towards the optimum.

For the head model a Virtual Population head model was used, which consists of eight highly detailed anatomical whole-body models of adults and children [34]. The models or numerical phantoms are based on high-resolution MR images of healthy volunteers. All of their approximately 80 organs and tissues are represented by three-dimensional CAD objects yielding a high level of detail. We choose the 11 year-old girl model. For the 2D case a thin layer of the brain with 1 *mm* resolution was selected which has 16 004 dofs and 10 tissues, i.e., grey matter, white matter, connective tissue, marrow red, blood vessels, CSF, cerebellum, fat,

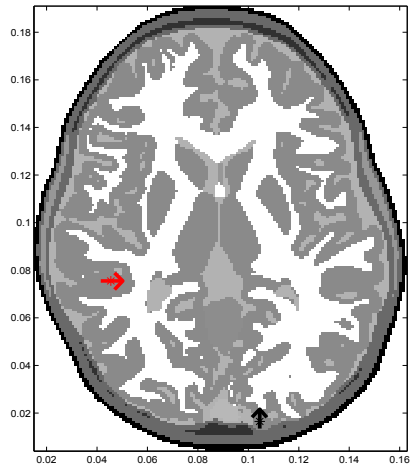

Figure 6.1: Position and orientation of the spike and background sources in 2D, (Red arrow: spike source, Black arrow: background source).

skull and scalp. Thirty equally distant EEG electrodes were used to measure the potential values on the scalp. In the 3D case the girl's head model had 2 *mm* resolution with 394 255 dofs and 22 tissues. The 81 EEG electrodes were placed on the head surface based on the 10/10 EEG electrode system [35]. The conductivity values were taken from a database [36].

6.1.1 2D Simulation

For generating the synthetic EEG data in the test cases two dipole sources are placed inside the brain, see Figure 6.1. Source 1 intended to resemble the spike pulse and was simulated with a half sinusoidal signal with 30 *ms* duration. Source 2 corresponded to the lower-amplitude background activity given by a sinusoidal signal with 100 *ms* duration. In the forward problem the EEG potential at the electrode positions are calculated from the sources. Then, the peak value of the potential is used as input to the inverse problem to estimate the position and orientation of the spike source, Figure 6.2 and 6.3 show the potential and electric field inside the model generated by the sources at the peak time, respectively. One can see that the both sources are active in the peak time. In Figure 6.3, we normalized the electric field that help to understand the electric field flow more clearly.

In order to validate the solution of the inverse problem, the position and the orientation errors are defined as the distance and angle between the estimated dipoles and the actual sources. Number of evaluations were equal to 350 for all three methods and they had same initial points. For SPSO the number of particles

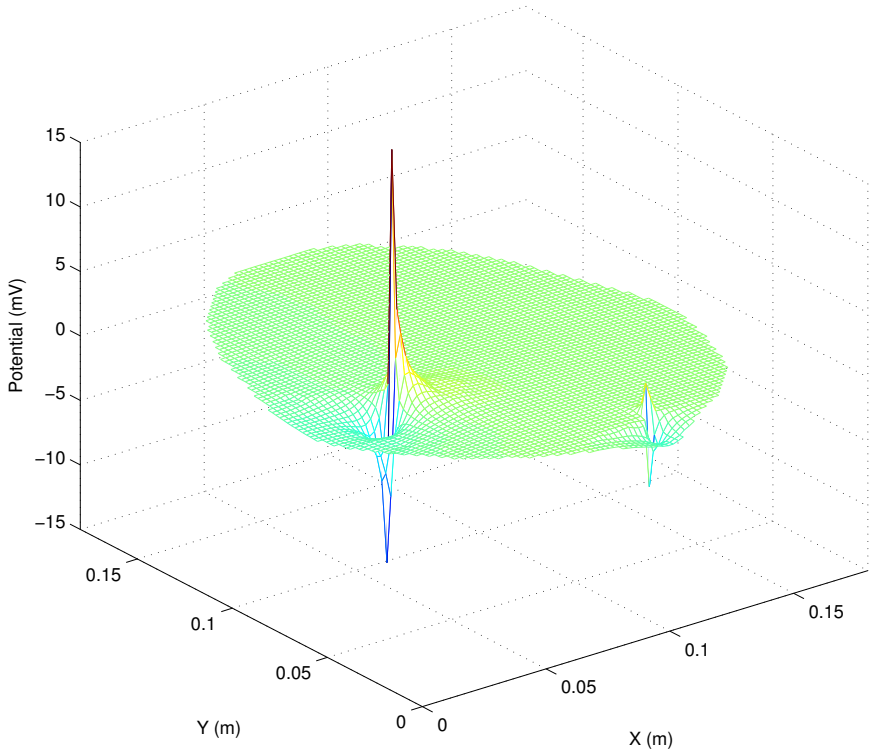

Figure 6.2: Potential generated by sources at the peak time in the 2D model.

was 30 and $c_1 = c_2 = 2.05$. Table 6.1 presents localization error results averaged for 10 run, relative error and also orientation errors for the best value found in the last evaluation. Since the DIRECT does not have any random parameters the same result was obtained for all runs. As can be seen from Table 6.1 the position and orientation of the source estimated by MPSO is very close to the real source. In this case DIRECT and SPSO has larger LE and OE because of trapping in a local minima and might need more evaluations to converge to the global minima. Figure 6.4 shows a RE curve to illustrate the convergence of the methods. Because of simulating two dipoles in the forward problem and estimating one in the inverse problem the relative error never reach the zero and it always has a constant offset which here is equal to 0.48. More complicated 2D cases and as well as a 3D case are presented in Paper **I**.

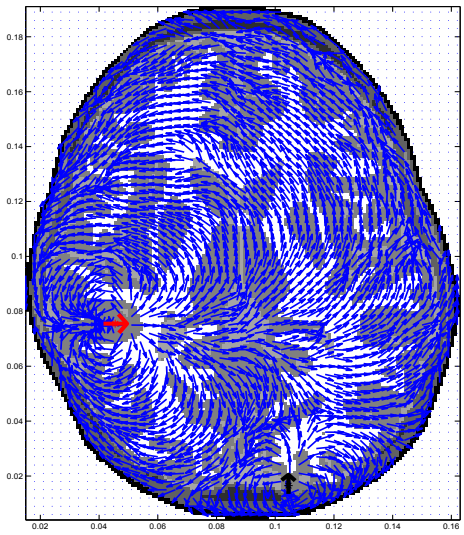

Figure 6.3: Electric field generated by sources at the peak time in the 2D model.

Table 6.1: Comparison between standard PSO, modified PSO and DIRECT in the 2D case. The results are averaged after 10 runs, where 'LE(mean)' is the localization error average and 'std' stands for standard deviation. 'RE' and 'OE' are the relative error and orientation error for the best run found in the last generation.

Method	LE(mean$\pm$std[mm])	RE	OE([deg])
MPSO	0.7$\pm$0.39	0.49	0.04
SPSO	5.08$\pm$3.0	0.56	7.73
Direct	7.5	0.63	18.8

6.2 Clinical Test

The T1-weighted MR data of the subject's head was generated on a 1.5T Philips by the Department of clinical neurophysiology at Sahlgrenska University Hospital, Göteborg, Sweden. The resolution of each voxel in the MR data is 1x1x1 *mm*. The segmentation of the five tissues was done by FSL [37, 38] in two steps. In a first step, mask of skin, skull and brain was generated by using the intensity threshold value 0.5 in BET module [39]. In a second step, automated segmentation of three tissues i.e., cerebrospinal fluid (CSF), white matter and grey matter, of the brain were performed by applying the FAST module [40]. The segmented tissues were checked and corrected manually by a clinical expert. Here the high

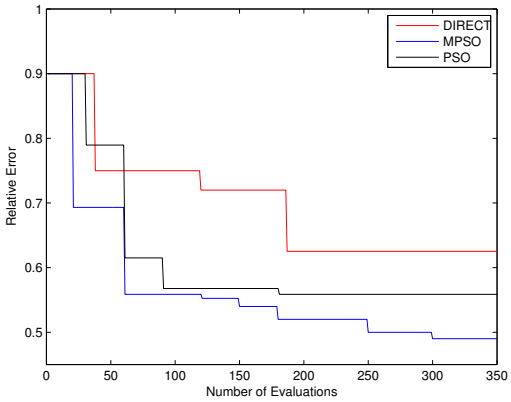

Figure 6.4: Comparison of the best solution trajectories of 10 runs between the standard PSO, modified PSO and DIRECT.

resolution model is necessary to model the CSF compartment and the thin area of the skull. This accurately resulted in a 1x1x1 *mm* FE head model.

The following conductivities were then assigned to the FE compartments based on their segmentation labels for the isotropic reference model [41, 42, 43, 44]: skin = 0.43 S/m, skull = 0.0042 S/m (skull to skin conductivity ratio of approximately 1:100), CSF = 1.538 S/m, gray matter = 0.33 S/m, and white matter = 0.142 S/m.

The 61 EEG electrodes were placed on the subject head's based on the 10/10 EEG electrode system [35]. The 3D (-x,-y,-z) coordinates of these electrodes were measured before and after the SEP stimulation experiment with a digitizer and for the electrode registration three reference points, i.e., nasion (the delve at the top of the nose, level with the eyes), left tragus (small point situated in front of the left concha) and right tragus (small point situated in front of the right concha) were measured on the subject's head as well. By using an affine transformation, the measured points were co-registered to the head model surface.

Evoked potentials are the electrical signals generated by the nervous system in response to sensory stimuli. Auditory, visual, and somatosensory stimuli are used commonly for clinical evoked potential studies. Somatosensory evoked potentials (SEP) consist of a series of waves that reflect sequential activation of neural structures along the somatosensory pathways. Sensory nerves (cell bodies in the dorsal root ganglia) transmit the signal rostrally and ipsilaterally (first order fibers), in the posterior column to a synapse in the dorsal column nuclei at the cervicomedullary junction [45]. Then the signal is passed via the second order fibers that cross to the contralateral thalamus via the medial lemniscus. Finally, the signal travels via the third order fibers from the thalamus to the frontoparietal sensory cortex. While SEP can be elicited by mechanical stimulation, clinical studies use electrical stim-

ulation of peripheral nerves, which gives larger and more robust responses. The stimulation sites typically used for clinical diagnostic SEP studies are the median nerve at the wrist, the common peroneal nerve at the knee, and/or the posterior tibial nerve at the ankle.

Rapid stimulus delivery rates should be avoided, as they degrade the SEP waveforms. We used one stimuli per second is our measurements. One should notice that the rates that are exact subharmonics of the line frequency (eg, 5.0 Hz) should be avoided, since their use would lead to contamination of the averaged SEP by large artifacts of the line frequency (50 or 60 Hz). To increase the SNR signal averaging were used. On-line artifact rejection was used to prevent epochs with unusually high noise levels from contaminating the averages. SEP components typically are named by their polarity and typical peak latency in the normal population. For example, N20 is a negativity that typically peaks at 20 milliseconds after the stimulus. the N20 predominantly reflects activity of neurons in the hand area of the primary somatosensory cortex [46] and we use this potential as input for the inverse problem. Paper **II** presents the results for this clinical test.

CHAPTER 7

Contribution and Future Work

This chapter consist of two parts. One part is the summary of the papers and the other is discussion about possible future work.

7.1 Papers

A brief summary of the papers, appended to this thesis, is given below.

Paper I Application of Particle Swarm Optimization in Epileptic Spike EEG Source Localization

A modified version of a PSO algorithm to solve EEG source localization is presented in this paper. The modified PSO proposed here uses the velocity update properties from the original PSO, ideas from evolutionary programming and a new property called authority. The new proposed method was tested for synthetic EEG data. The results from the synthetic data showed that the modified PSO algorithm can find the optimal solution significantly faster and more accurate than the standard PSO and also reduce the probability of trapping in local minima. The proposed modified PSO can also be implemented in a parallel computing environment making the inverse problem solution very cheap. One significant advantage of our method is that the algorithm could be modified, varied or extended according to the problem constraints and is also very flexible to partial changes during

the inverse problem e.g., moving direction, selection schemes, mutation and evolutionary operations.

Paper II A Clinical Study of EEG Source Localization: Somatosensory Evoked Potential

In this paper, the ability of the modified PSO method was tested for EEG source localization by using the clinical data. Somatosensory evoked potentials (SEPs) stimulation by an electrical pulses on the median nerve of a healthy subject, were recorded with 61 EEG electrodes placed on the scalp. For the forward problem, we built a realistic high-resolution finite element head volume conductor based on a T1-weighted MR data set for the construction of a five-tissue model, i.e., grey matter, white matter, CSF, skull and skin. Based on a clinical expert the x- and y-coordinates of the estimated source are correctly located but the z- coordinate is a little deeper than expected.

7.2 Future Work

7.2.1 Segmentation Error

In the clinical test we have used the brain segmentation tool, i.e., FSL for the five tissues classification (grey matter, white matter, CSF, skull and skin) in order to construct a patient-specific head model. While this segmentation is not perfect we can expect error in the source localization results. In the experimental analysis with synthetic brain segmentation, we have seen that the performance of FSL for the grey matter and white matter classification is reasonable while for the CSF, which is very important tissue in the forward problem, skin and skull is not satisfactory. Other issue is motion artifacts in the MRI data that increase the segmentation error. In next clinical try, in order to overcome this problem, we are planning to take more modalities of high resolution MR image, e.g, T1-T2/PD MRI and also aiming to apply other robust techniques for MRI segmentation.

7.2.2 Anisotropic Tissue Conductivity

The cerebrospinal fluid (CSF) compartment is known to have a much higher conductivity than brain's gray and white matter and moreover the skull is often considered to be an anisotropic (different conductivity values in different space directions) conductor because of its three-layeredness into top and bottom compacta and spongiosum. Furthermore, conductivity anisotropy with a ratio of about 1 to

9 (normal to parallel fibers) has been measured for brain white matter. The robust and non-invasive direct in-vivo measurement of brain conductivity anisotropy is not possible. However, there is an assumption that the conductivity tensor shares the eigenvectors with the water diffusion tensor (DT), which can be measured non-invasively by means of DT-MRI. Using the DT-MRI modality for extracting the tissue conductivity tensors and adding these new information might built a more accurate patient-specific head model for the EEG source localization.

7.2.3 Reciprocity Theorem

Two approaches have been described for computing the EEG lead-field with a number of forward simulations equal to the number of measurement rows, rather than the number of source columns. One of these approaches is based on linear-algebraic manipulations of the forward problem, and the other approach is based on principle of electric reciprocity. As explained in Chapter 3, the linear-algebraic manipulations was used for the forward problem in this work. The theory of reciprocity was already introduced in 1853 by Helmholtz and was intensively studied for both the electric and the magnetic cases. The reciprocity theorem for the electric case states that the field of the so-called lead vectors is the same as the current field raised by feeding a reciprocal current to the lead. One possible future work is to apply the reciprocity theorem on the forward problem to calculate the lead-field and then compare the results of the source localization from this lead-field with the one from linear-algebraic manipulations method which is used in this work. As far as we know, it is not yet clear which one of these methods is more accurate and efficient to use for the epileptic spike source localization in the clinical study.

Bibliography

[1] D. L. Kraeme, M. E. Brandling-Bennett, and D. G. Vossler. Epilepsy surgery. *Medscape reference, Drug, Diseases and Procedures*, 2011.

[2] J. Engel, S. Wiebe, J. French, M. Sperling, P. Williamson, D. Spencer, R. Gumnit, C. Zahn, E. Westbrook, and B. Enos. Practice parameter: Temporal lobe and localized neocortical resections for epilepsy. *Epilepsia*, 44(6):741–751, 2003.

[3] S. Spencer, A.T. Berg, B.G. Vickrey, M.R. Sperling, C.W. Bazil, S. Shinnar, J.T. Langfitt, T.S. Walczak, S.V. Pacia, N. Ebrahimi, and D. Frobish. Initial outcomes in the multicenter study of epilepsy surgery. *Neurology*, 61(12):1680–1685, 2003.

[4] J.S. Ebersole. Defining epileptogenic foci: Past, present, future. *Clin. Neurophysiol.*, 14:470–483, 1997.

[5] Q. Chen and S. Lui. MRI-negative refractory partial epilepsy: Role for diffusion tensor imaging in high field MRI. *Epilepsy Research*, 80:83–89, 2008.

[6] J. C. De Munck. The potential distribution in a layered anisotropic spheroidal volume conductor. *Journal of Applied Physics*, 64(2):464–470, 1988. Cited By (since 1996): 77.

[7] S. van den Broeh, H. Zhou, and M. Peters. Computation of neuromagnetic fields using finite-element method and Biot-Savart law. *Medical and Biological Engineering and Computing*, 34(1):21–26, 1996.

[8] F. Edelvik, B. Andersson, S. Jakobsson, S. Larsson, M. Persson, and Y. Shirvany. An improved method for dipole modeling in EEG-based source localization. In *World Congress on Medical Physics and Biomedical Engineering*, volume 25 of *IFMBE Proceedings*, pages 146–149. 2009.

[9] H. Hallez, B. Vanrumste, R. Grech, J. Muscat, W. De Clercq, A. Vergult, Y. D'Asseler, K. P. Camilleri, S. G. Fabri, S. Van Huffel, and I. Lemahieu. Review on solving the forward problem in EEG source analysis. *Neuroengineering and Rehabilitation*, 46(4), 2007.

[10] C. M. Michel, M. M. Murray, G. Lantz, S. Gonzalez, L. Spinelli, and R. Grave de Peralta. EEG source imaging. *Clinical Neurophysiology*, 115(10):2195–2222, 2004.

[11] H. L. Attwood and W. A. MacKay. *Essentials of Neurophysiology*. B. C. Decker, Hamilton, Canada, 1989.

[12] L.G. Kiloh, A.J. McComas, J.W. Osselton, and A.R.M. Upton. *Clinical Electroencephalography*. 1981.

[13] H. Gray. *Gray's Anatomy*. Longman Group Ltd, 1973.

[14] S. Sanei and J.A. Chamers. *EEG Signal Processing*. John Wiley and Sons Ltd,, 2007.

[15] E. Niedermeyer and Da Silva F. Lopes. *Electroencephalography Baltimore*. Williams and Wilkins, 1993.

[16] R.M. Gulrajani. *Bioelectricity and Biomagnetism, chap Electroencephalography*. John Wiley and Sons, Inc, 1998.

[17] K. X. Charand. `http://hyperphysics.phy-astr.gsu.edu/hbase/biology/actpot.html`.

[18] S. Baillet, J.C. Mosher, and R.M. Leahy. Electromagnetic brain mapping. pages 14–30, 2001.

[19] M. Scherg and D. von Cramon. Two bilateral sources of the late AEP as identified by a spatio-temporal dipole model electroencephalogr. *Clin. Neurophysio.*, pages 32–44, 1985.

[20] Y. Okada. Neurogenesis of evoked magnetic fields biomagnetism. *ed S. N. Erne, H. D. Hahlbohm and H. Lübbig*, pages 399–408, 1981.

[21] J. C. de Munck, B. W. van Dijk, and H. Spekreijse. Mathematical dipoles are adequate to describe realistic generators of human brain activity. *IEEE Trans. Biomed. Eng.*, 35:960–966, 1988.

[22] P. Nunez. Localization of brain activity with electroencephalography advances in neurology. *Magnetoencephalography*, 54:39–65, 1990.

[23] H. Buchner, G. Knoll, M. Fuchs, A. Rienäcker, R. Beckmann, M. Wagner, J. Silny, and J. Pesch. Inverse localization of electric dipole current sources in finite elementmodels of the human head electroencephalogr. *Clin. Neurophysiol.*, 102:267–268, 1997.

[24] R. Grech, T. Cassar, J. Muscat, K. P. Camilleri, S. G. Fabri, M. Zervakis, P. Xanthopoulos, V. Sakkalis, and B. Vanrumste. Review on solving the inverse problem in EEG source analysis. *Journal of NeuroEngineering and Rehabilitation*, 5, 2008.

[25] R. Eberhart and J. Kennedy. A new optimizer using particle swarm theory. In *Micro Machine and Human Science, 1995. MHS '95., Proceedings of the Sixth International Symposium on*, pages 39 –43, 1995.

[26] J. Kennedy and R. Eberhart. Particle swarm optimization. In *Neural Networks, 1995. Proceedings., IEEE International Conference on*, volume 4, pages 1942 –1948 vol.4, 1995.

[27] Y. Shi and R. Eberhart. A modified particle swarm optimizer. In *Evolutionary Computation Proceedings, 1998. IEEE World Congress on Computational Intelligence., The 1998 IEEE International Conference on*, pages 69 –73, 1998.

[28] Y. Shi and R. C. Eberhart. Parameter Selection in Particle Swarm Optimization. In *EP '98: Proceedings of the 7th International Conference on Evolutionary Programming VII*, pages 591–600, London, UK, 1998. Springer-Verlag.

[29] M. Clerc. The swarm and the queen: towards a deterministic and adaptive particle swarm optimization. In *Evolutionary Computation, 1999. CEC 99. Proceedings of the 1999 Congress on*, volume 3, 1999.

[30] R.C. Eberhart and Y. Shi. Comparing inertia weights and constriction factors in particle swarm optimization. In *Evolutionary Computation, 2000. Proceedings of the 2000 Congress on*, pages 84 –88 vol.1, 2000.

[31] M. Clerc. Think locally, act locally: The way of life of cheap-pso, an adaptive pso. 2001.

[32] K. B Lee and J. H. Kim. Particle swarm optimization driven by evolving elite group. In *Evolutionary Computation, 2009. CEC '09. IEEE Congress on*, pages 2114 –2119, 2009.

[33] D. R. Jones, C. D. Perttunen, and B. E. Stuckman. Lipschitzian optimization without the lipschitz constant. *Journal of Optimization Theory and Applications*, 79:157–181, 1993.

[34] `http://www.itis.ethz.ch/services/human-and-animal-models/human-models/`.

[35] V. Jurcak, D. Tsuzuki, and I. Dan. 10/20, 10/10, and 10/5 systems revisited: Their validity as relative head-surface-based positioning systems. *NeuroImage*, 34(4):1600 – 1611, 2007.

[36] P.A. Hasgall, E. Neufeld, M.C. Gosselin, A. Klingenböck, and N. Kuster. IT'IS database for thermal and electromagnetic parameters of biological tissues. 2011.

[37] Mark W. Woolrich, Saad Jbabdi, Brian Patenaude, Michael Chappell, Salima Makni, Timothy Behrens, Christian Beckmann, Mark Jenkinson, and Stephen M. Smith. Bayesian analysis of neuroimaging data in FSL. *NeuroImage*, 45:S173 – S186, 2009.

[38] Stephen M. Smith, Mark Jenkinson, Mark W. Woolrich, Christian F. Beckmann, Timothy E.J. Behrens, Heidi Johansen-Berg, Peter R. Bannister, Marilena De Luca, Ivana Drobnjak, David E. Flitney, Rami K. Niazy, James Saunders, John Vickers, Yongyue Zhang, Nicola De Stefano, J. Michael Brady, and Paul M. Matthews. Advances in functional and structural MR image analysis and implementation as FSL. *NeuroImage*, 23:S208 – S219, 2004.

[39] S. M. Smith. Fast robust automated brain extraction. *Human Brain Mapping*, 17(3):143–155, 2002.

[40] Y. Zhang, M. Brady, and S. Smith. Segmentation of brain MR images through a hidden markov random field model and the expectation-maximization algorithm. *Medical Imaging, IEEE Transactions on*, 20(1):45 –57, 2001.

[41] J. Haueisen, D.S. Tuch, C. Ramon, P.H. Schimpf, V.J. Wedeen, J.S. George, and J.W. Belliveau. The influence of brain tissue anisotropy on human EEG and MEG. *NeuroImage*, 15(1):159 – 166, 2002.

[42] K.R. Foster and H.P. Schwan. Dielectric properties of tissues and biological materials: a critical review. *Crit Rev Biomed Eng*, 17(1):25 – 104, 1989.

[43] L. A. Geddes and L. E. Baker. The specific resistance of biological materials: A compendium of data for the biomedical engineer and physiologist. *Med. Biol. Eng. Comput.*, 5:271 – 293, 1967.

[44] S. Gabriel, R.W. Lau, and C. Gabriel. The dielectric properties of biological tissues: III parametric models for the dielectric spectrum of tissues. *Phys Med Biol*, 41(11):2271 – 2293, 1996.

[45] K.S. Saladin. *Anatomy and Physiology*. McGraw-Hill, New York, 2004.

[46] M. J. Aminoff. *Electrodiagnosis in Clinical Neurology*. Churchill Livingstone, Elsevier, 2005.